Electrohydrodynamics of rigid macromolecules with permanent and induced dipole moments. II

M. H. Kwon and O. O. Park

Department of Chemical Engineering, Korea Advanced Institute of Science and Technology, 373-1, Kusong-dong, Yusong-gu, Taejon, 305-701, Korea

(Received 2 January 1991; accepted 23 January 1992)

Synopsis

The orientation distribution of rigid macromolecules dissolved at low concentration in a dielectric Newtonian fluid is solved for the case in which simultaneous hydrodynamic and electric fields are applied. Macromolecules are taken to be Brownian rigid spheroids of arbitrary aspect ratio and both permanent and induced dipole moments are included. To solve the problem with arbitrary strength of fields, the Galerkin method based on spherical harmonics is adopted. The converged solutions are used in the prediction of the steady state birefringence and extinction angle over very wide ranges of field strengths. Due to the coupled effects of flow and external field, somewhat complicated responses are predicted and saturation features are revealed at the strong flow limit. External field dependence due to the induced dipole is similar to that of the permanent case for most field conditions. Finally, it is shown, taking poly-γ-benzyl-L-glutamate solutions with various molecular weights as an example, how results in this article are applicable to an analysis of a real system.

INTRODUCTION

Electrohydrodynamic research on polymeric liquids involving nonspherical particles with electric dipoles have been steadily performed together with the advance of relevant theories and experimental techniques. The present work, as a continuation of the previous work reported by Park (1988), will consider the solutions of Brownian rigid macromolecules with arbitrary aspect ratio dissolved in a dielectric Newtonian fluid over entire ranges of the combined electric and hydrodynamic fields. Both induced and permanent dipole moments are in-

cluded. The key difference from the previous work is coverage of a full range of the combined field strengths extended to the saturation strengths.

Even without the complicating effect of the external couples and even after restriction to dilute solutions, a complete quantitative description of the system is a formidable task. The major difficulty arises when one would like to solve the diffusion equation that governs the distribution of orientations. Analytical solutions are not available and perturbation solutions, obtained after considerable effort, yield results which are valid only over a limited range.

Okagawa and co-workers (1974) have considered most questions pertaining to large, non-Brownian particles at infinite dilution subjected to electric and hydrodynamic fields. Ikeda (1963) and Mukohata and co-workers (1962) have already studied the steady state response of rodlike polymer chains with assumed permanent and induced dipole moments subject to weak electrohydrodynamic field. Starting from the results of Okagawa *et al.* in order to include the effects of Brownian motions, Park developed the more systematic perturbation solution procedure by utilizing the standard Fokker–Planck formulation. Leal and Hinch (1971, 1972) calculated singular perturbation solutions for strong flows and weak diffusion and later gave perturbation solutions for near spheres.

Stewart and Sørensen (1972) presented numerical solutions for the steady state problem over the wide range of Peclet numbers for rigid dumbbell suspensions in steady shear using Galerkin's method. Thenceforth their typical approach to the strong field problem has been applied to variously extended problems. Strand *et al.* (1987) studied the transient response of suspensions of rigid rods after inception of steady shear flow. Using Galerkin's method in the spatial coordinates and the spectral method in time, they have obtained numerical solutions up to high Peclet numbers ($P_\lambda = 10$, i.e., the dimensionless shear rate $G/D_r = 60$). Kamiyama and Satoh (1989) analyzed the rheological properties of magnetic fluids in case of a steady shear flow in a strong magnetic field perpendicular or parallel to a shearing plane. They used a needlelike cluster model in which the particles in magnetic fluids form rigid linear aggregates to make clusters.

We have analyzed the steady state governing equation for the orientation distribution function, which belongs to the class of Fokker–Planck equations, by Galerkin's method. After using the specially designed numerical scheme and applying the operators in prior work by Park, the matrix reduced from the governing equation could be band-

edly diagonalized and the system of equations can be solved very efficiently. This article contains the strong field problems considering the entire ranges of simultaneous electric and hydrodynamic fields. In addition, both the external couples, induced and permanent dipole, are explored and distinct from each other. The solutions obtained are applied to the calculation of birefringence and extinction angle and discussions on the predictions of optical properties are presented.

GOVERNING EQUATIONS

This article is based on the previous paper by Park and practically starts from their governing Eqs. (8) and (9). However for a more reasonable interpretation of the problem, the dimensionless parameters β and γ^2 related to the electric field should be modified. For a connection with the previous work and clear circumstances, we first cite a model system using the following assumptions.

(1) The solvent is a Newtonian homogeneous isotropic fluid of dielectric constant K_2.

(2) Brownian solute particles of dielectric constant qK_2 are dissolved dilutely and approximated as rigid, neutrally buoyant, prolate spheroids of revolution in which $2a$ and $2b$ are lengths of major and minor axes.

(3) An isolated nonelectrolytic particle without any interaction between particles is considered.

(4) The external field is composed of both simple shear flow field ($V_x = Gy$) and uniform electrostatic field E_0 perpendicular to the shear direction.

(5) Solute particles have either permanent dipole moments in the direction of their symmetry axes or induced dipole moments under the external electric field.

For the above model system, the normalized diffusion equation expressed in terms of operators related to respective fields describe the evolution of the orientation distribution function N,

$$6\frac{\partial N}{\partial \tau} + \alpha\Omega_1(N) + \beta\Omega_3(N) + \gamma^2\Omega_2(N) = \Lambda(N), \tag{1}$$

with the normalization condition for N,

$$\int_0^{\pi} d\theta \sin\theta \int_0^{2\pi} d\phi\, N = 1. \tag{2}$$

The operator Ω_1 is due to the shear flow. The operators Ω_2 and Ω_3 are due to the induced and permanent dipole moments of the spheroids responding to the electric field. The differential operator Λ is simply the angular part of the Laplacian operator in the spherical coordinates, defined as in Bird *et al.* (1987). These operators and their properties have already been expressed by spherical functions in the previous paper. The geometric symmetry condition for N disappears when spheroidal particles have any finite permanent dipoles.

Rotational diffusivity D_r and dimensionless shear rate α, and dimensionless field parameters β and γ^2 related to the permanent and induced moments are given by

$$\alpha = G/D_r \quad D_r = \frac{3kT}{4\pi a^3 \eta_0} r^2 Q(r), \tag{3}$$

$$\beta = \frac{VB_a \mu_0 E_0}{kT}, \tag{4}$$

$$\gamma^2 = -\frac{V\epsilon_0 K_2 P(q,r) E_0^2}{kT}. \tag{5}$$

Here r is the aspect ratio of spheroids and $Q(r)$ is the geometric factor given by Okagawa *et al.* which can be approximated as

$$r^2 Q(r) = [\ln(2r) - 0.5]/2, \quad r > 2.$$

η_0 is the viscosity of the Newtonian fluid, $V(=\frac{4}{3}\pi ab^2)$ is the volume of a prolate spheroid, μ_0 is the permanent dipole moment per unit volume of a spheroid, ϵ_0 is the permittivity of a vacuum, and B_a is the internal field function (O'Konski, 1976).

Most of the other formulas and nomenclature used earlier are also valid and thus available in the present work, but a few were altered. Though the above β and γ^2 can be expressed into the forms given in the previous paper, present definitions are more reasonable in the physical and practical sense. In addition, $P(q,r)$ of Eq. (5) differs from that of Park and Okagawa *et al.* by a multiplying factor $\{-[1/2Q(r)]\}$.

SOLUTION PROCEDURE BY GALERKIN'S METHOD

Since it is difficult to obtain an analytic solution of the governing Eqs. (1) and (2), Galerkin's method is used to get the approximate solution.

We use spherical harmonics of the first $M+1$ kinds to construct an Mth-order approximation to N, denoted by $N^{(M)}$:

$$N^{(M)} = \sum_{n=0}^{M} \sum_{m=0}^{n} (A_n^m P_n^m c_m + B_n^m P_n^m s_m), \tag{6}$$

in which P_n^m are the associated Legendre functions and c_m and s_m denote $\cos m\phi$ and $\sin m\phi$, respectively. The coefficients A_n^m and B_n^m are functions of α, β, γ^2, and R defined by $(r^2-1)/(r^2+1)$. These coefficients are to be determined for each approximation $N^{(M)}$ so as to make it close to the actual N in some sense. To find the coefficients at the Mth level of approximation, we insert Eq. (6) into Eq. (1) and use the general relationships of the operators given in Appendixes A, B, C, and Eq. (17) of the previous paper. Here only the steady state solution is considered:

$$\begin{aligned}
&\sum_{n=0}^{M} \sum_{m=0}^{n} \Bigg(n(n+1)(A_n^m P_n^m c_m + B_n^m P_n^m s_m) \\
&\quad - \alpha \sum_{p=1}^{3} \sum_{q=1}^{3} a_{n,n+2q-4}^{m,m+2p-4} (A_n^m P_{n+2q-4}^{m+2p-4} s_{m+2p-4} \\
&\quad - B_n^m P_{n+2q-4}^{m+2p-4} c_{m+2p-4}) + \beta \sum_{p=1}^{2} \sum_{q=1}^{2} b_{n,n+2q-3}^{m,m+2p-3} \\
&\quad \times (A_n^m P_{n+2q-3}^{m+2p-3} s_{m+2p-3} - B_n^m P_{n+2q-3}^{m+2p-3} c_{m+2p-3}) \\
&\quad + \gamma^2 \sum_{p=1}^{3} \sum_{q=1}^{3} c_{n,n+2q-4}^{m,m+2p-4} (A_n^m P_{n+2q-4}^{m+2p-4} c_{m+2p-4} \\
&\quad + B_n^m P_{n+2q-4}^{m+2p-4} s_{m+2p-4}) \Bigg) = F^{(M)},
\end{aligned} \tag{7}$$

where $F^{(M)}$ is the residual function in the Mth-order approximation. Equations to determine A_n^m and B_n^m are obtained from the requirement that they must be orthogonal to all spherical harmonics of order less than or equal to M:

$$q(q+1)A_q^p + \sum_{n=0}^{M}\sum_{m=0}^{n}(\alpha a_{n,q}^{m,p}B_n^m - \beta b_{n,q}^{m,p}B_n^m + \gamma^2 c_{n,q}^{m,p}A_n^m) = 0,$$

$$q(q+1)B_q^p - \sum_{n=0}^{M}\sum_{m=0}^{n}(\alpha a_{n,q}^{m,p}A_n^m + \beta b_{n,q}^{m,p}A_n^m + \gamma^2 c_{n,q}^{m,p}B_n^m) = 0$$

$$(p = 0,1,2,\ldots,q; \quad q = 0,1,2,\ldots,M, \text{ except } p = q = 0). \tag{8}$$

Now we have the algebraic equations suitable for the numerical computation. This equation can be simplified more. First, A_0^0 is obtained from the normalization condition Eq. (2):

$$A_0^0 = 1. \tag{9}$$

None of the coefficients B_n^0 are required, since the terms with those are identically zero. The symmetry in the flow field requires that A_n^m and B_n^m are zero for either odd m or odd n. This symmetry requirement is kept even though spheroidal particles are to have the induced dipoles. But the permanent dipole restricts the simplification of the problem. Because of the properties of the operator Ω_3 due to the permanent dipole, A_n^m and B_n^m are zero only when $m + n$ is odd. A special care must be taken in cases of $m = 1$ when calculating the coefficients of Ω_1 and Ω_2 in relation to Ω_3. The problem is thus to determine the remaining $M(M+3)/2$ coefficients.

BIREFRINGENCE AND EXTINCTION ANGLE

Birefringence Δn is defined as the difference in the principal values of the real part of the refractive index tensor in the plane orthogonal to the propagation axis of the light and the extinction angle χ as the orientation of the principal axis of the refractive index tensor with respect to a laboratory frame (Johnson *et al.*, 1985). If the light is propagating along the z axis, the birefringence and the extinction angle are

$$\Delta n = C(\langle P_2^2 c_2\rangle^2 + \langle P_2^2 s_2\rangle^2)^{1/2}, \tag{10}$$

$$\tan(2\chi) = \langle P_2^2 s_2\rangle / \langle P_2^2 c_2\rangle. \tag{11}$$

Here C is a constant which is related to the molecular properties such as concentration of the molecules, optical polarizabilities of molecules, etc. It is instructive to express C for a dilute solution of the modeled rigid macromolecules. C may be written as follows:

$$C = 2\pi\phi_v(g_a - g_b)/n_o, \tag{12}$$

where ϕ_v is the volume fraction of the particles, n_o is the refractive index of the solvent, and $(g_a - g_b)$ is the optical anisotropy factor.

Since these bulk solution properties are averaged over the distribution function (as indicated by the angular brackets $\langle\ \rangle$), birefringence and extinction angle can be evaluated once the distribution function is known. The expressions for the above averages may be written explicitly in terms of A_n^m and B_n^m by using the orthogonality property of the spherical harmonics. The results are simply written as

$$\langle P_2^2 c_2 \rangle = \tfrac{12}{5} A_2^2, \tag{13a}$$

$$\langle P_2^2 s_2 \rangle = \tfrac{12}{5} B_2^2. \tag{13b}$$

NUMERICAL STRATEGY

Our numerical strategy is basically an extension of the approach used by Stewart and Sørensen. Numerical solutions could be obtained over a wide range of all dimensionless parameters. For any given values of α, β, γ^2, and R, the coefficients in $N^{(M)}$ are determined for successively larger values of M until both A_2^2 and B_2^2 converge to the relative error limit of 1×10^{-4}. In most cases the convergence condition was satisfied by taking 54 as the maximum value of M. Large values of M are needed for the strong field problems. Then the attempt to solve such problems becomes a formidable task, requiring the inversion step of a matrix of large size in which substantial computing time is consumed. To deal with such problems, a specially designed numerical algorithm is used.

The coefficient terms A_n^m and B_n^m with the smallest value of $m + n$ are first filled into a matrix and successively in order of magnitude of $m + n$. Among members with equal values of $m + n$, A_n^m and B_n^m with smaller values of n go first. Such ordering of terms A_n^m and B_n^m results in a diagonally banded matrix of which the maximum length is $2M + 2$ except in a case of $M = 2$. Inversion of this banded matrix is performed by back substitution following the lower decomposition scheme. This numerical algorithm drastically reduces the computation time and, in proportion to the reduced calculation steps, the truncation error decreases, too.

RESULTS AND DISCUSSION

It is well known that the birefringence Δn and the extinction angle χ are basic functions which determine the optical state of transparent materials. Through the above two functions, the model solution speci-

fied in the previous section is investigated. Shear and electric fields are applied simultaneously and both permanent and induced dipole moments are considered. A number of rigid macromolecules can be modeled as the prolate spheroid. Analyses in this work are also tentatively restricted to the cases of the prolate spheroid (that is, $R > 0$). They are, however, without any difficulties, equally applicable to the symmetric spheroid of revolution with any aspect ratio ranging from disklike ($R = -1$) to needlelike shape ($R = 1$). For such problems, in particular at strong fields extended to the saturated field, steady state solutions were obtained. In real calculations, all coefficients of A_n^m and B_n^m that determine the approximate probability density function $N^{(M)}$ are sought by solving the final algebraic Eq. (8) and the normalization condition Eq. (9). Only A_2^2 and B_2^2 among the above coefficients are used in calculating Δn and χ. In subsequent results, birefringence is given as a scale ($\Delta n/C$) divided by the constant C in Eq. (12).

The preliminary results at weak fields are presented in Fig. 1. The exact numerical solution by the Galerkin method was obtained within the convergence limit of 10^{-6}. Two perturbation solutions, Ikeda's second order and Park's fourth order, were compared with the exact numerical solution to check the correctness of the numerical work at weak fields. Figure 1 shows χ and Δn that respond to α varies from 0 to 5 at the weak electric field of $\beta^2 = \gamma^2 = 0.5$. We have already known from the previous study that respective dimensionless field parameters depend on α, β^2, and γ^2. As expected, the perturbation solutions nearly coincide with the exact one under weak fields in which the dimensionless governing parameters are smaller than unity. As α becomes larger than unity, the perturbation solutions deviate from the exact one and reveal a tendency to diverge according to respective perturbation orders. Though Fig. 1 shows the field dependence on α only, similar results were also obtained on β^2 and γ^2. Synergic effects in coupling fields in a range over weak field causes the perturbation solutions to diverge more rapidly as the fields are stronger. Therefore, the numerical results of the Galerkin method are required to cover the full ranges of field strengths.

Figures 2 and 3 show the steady optical state of the model solution over the full ranges of simultaneous shear and electric field strengths. Figure 2 are results in which permanent dipoles are considered. Results for cases of induced dipoles are seen in Fig. 3. In either figure, two cases of $R = 1$ ($r = \infty$; very slender rod) and $R = 0.6$ ($r = 2$; a slightly prolate spheroid) were compared in order to consider the geometric effect of solute particles. Results when the shear field only is applied are also plotted for a reference. Optical properties of the model solution varied

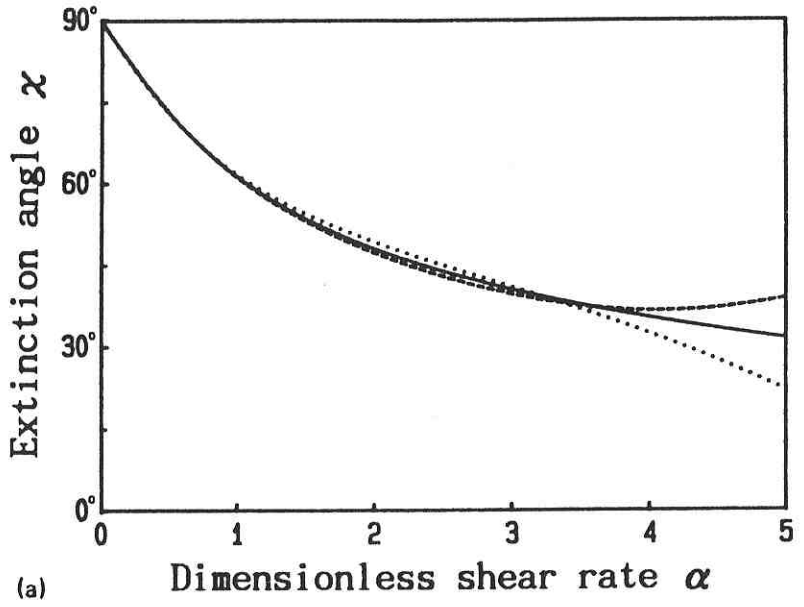

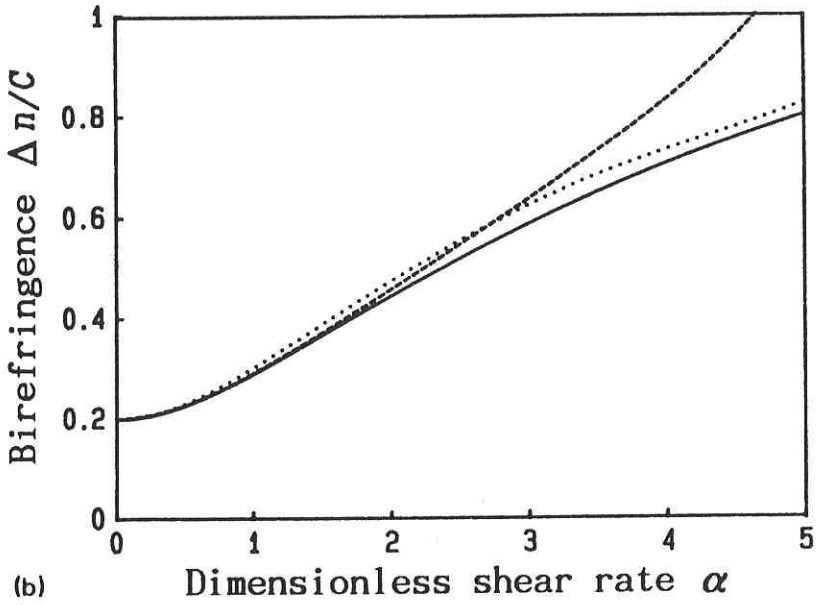

FIG. 1. Comparisons of (a) extinction angle χ and (b) birefringence $\Delta n/C$ for the converged numerical solution (—) and the perturbation solutions (– –, Park's fourth order; $\cdots$, Ikeda's second order). $R = 0.5$; α between 0 and 5; $\beta^2 = \gamma^2 = 0.5$, in which R is the aspect ratio parameter given by $(r^2 - 1)/(r^2 + 1)$, and β and γ^2 are dimensionless field parameters related to permanent and induced dipole moments, respectively.

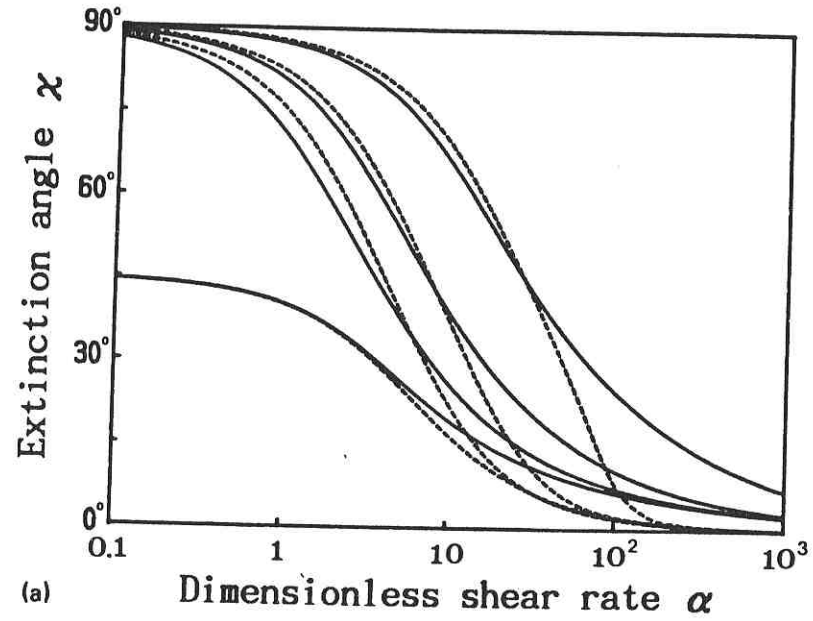

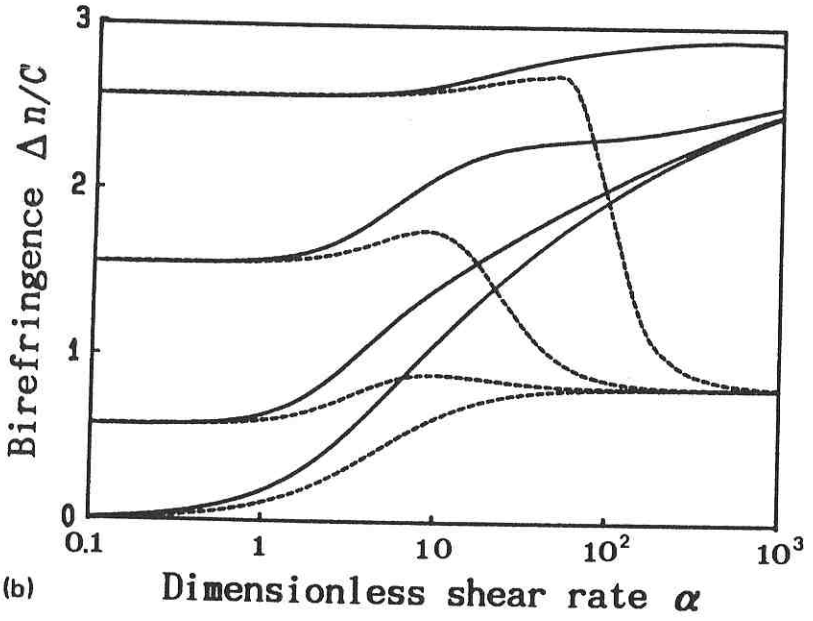

FIG. 2. Semilogarithmic representations of (a) extinction angle χ and (b) birefringence $\Delta n/C$ vs dimensionless shear rate α, when considering the permanent dipole moment only. In both figures, the solid curves are for aspect ratio parameter $R = 1$ and the dashed curves $R = 0.6$, and dimensionless permanent dipole strength $\beta = 0$, 2, 5, 20 from the bottom.

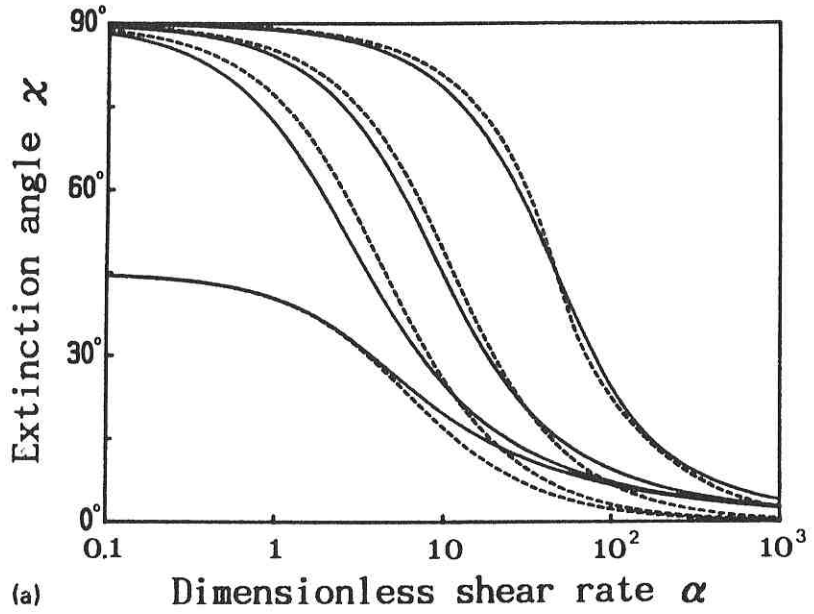

(a)

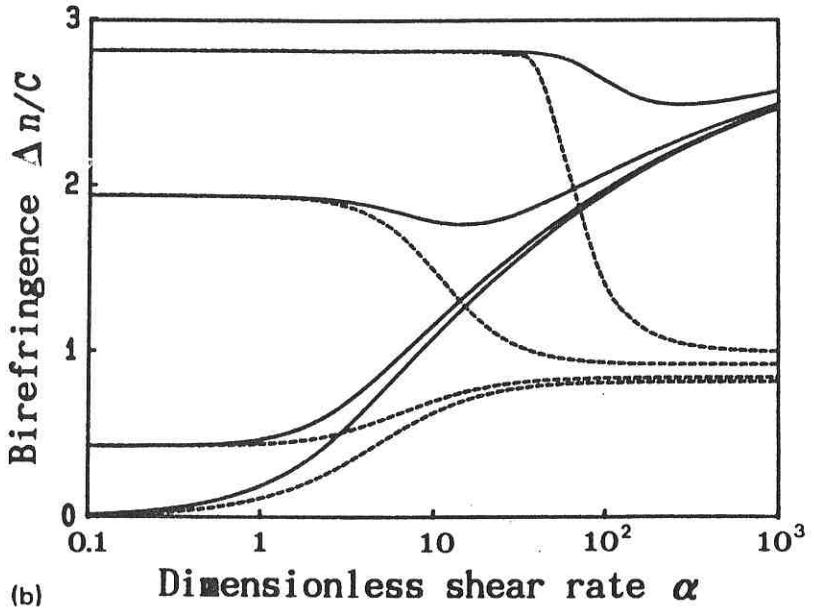

(b)

FIG. 3. Semilogarithmic representations of (a) extinction angle χ and (b) birefringence $\Delta n/C$ vs dimensionless shear rate α, when considering the induced dipole moment only. In both figures, the solid curves are for aspect ratio parameter $R = 1$ and the dashed curves $R = 0.6$, and dimensionless induced dipole strength $\gamma^2 = 0$, 2, 10, 50 from the bottom.

according to not only the absolute strengths of respective fields but also the relative strengths. Thus to interpret the results systematically the full ranges of the field strengths are divided into three regions as follows.

Region 1: The shear field is so weak that the electric field is relatively dominant. In both Figs. 2 and 3, the electric field acting perpendicularly to the shear direction will reduce the decrease of χ by offsetting the influence of α. Such a basic pattern of χ is continued in regions 2 and 3. Smaller R reduces the shear effect and makes it relatively easy for solute particles to align in the direction of the electric field. As a result, χ curves of $R = 0.6$ have slightly larger values than those of $R = 1$ in this region. It is important in an experimental view to notice that, at weak fields, χ responds very sensitively to the variation of the field strengths. In general, Δn increases as the applied field strength increases. A certain strength of electric field prevailing in this region keeps Δn nearly constant up to region 2 as seen in both figures. Unlike χ, Δn has little or no dependence on R only if the same field parameters are given. Some features in this region have already been known by earlier perturbation works valid at weak fields only. Region 1 includes, adaptively, those features of weak fields.

Region 2: Both shear and electric fields are considerably strong. The larger R is, the more effectively the electric field is swamped by a fairly strong shear flow. Thus, in both figures, χ for $R = 1$ decreases somewhat rapidly and two series of χ curves of $R = 0.6$ and 1 intersect in the middle of this region. For very slender particles with the permanent dipole, Δn increases, even though very gradually, as α increases. (See Fig. 2.) The slightly convex profile seen in the case of $\beta = 10$ is rather exceptional. Compared with the permanent dipole moments, the induced are swamped more easily. As seen in Fig. 3, all Δn curves with various values of γ^2 approach rapidly to the referred shear curve as α increases. In particular, when $R = 1$ and $\gamma^2 > 10$, Δn even decreases locally despite increasing α. For β or γ^2 over a certain value, Δn curves for small R deviate significantly from the results for $R = 1$ as α increases. All of the intermediate features in this region directly correspond to the appearance of rotary Brownian motion (RBM) caused by the fairly strong shear flow.

Region 3: The shear field is so very strong that the electric field is swamped significantly by RBM. This region is characterized by the saturated states revealed near extreme strengths of the coupled field. Though the electric field belonging to this region is so strong, it is significantly swamped by RBM owing to much stronger shear flow. Both Figs. 2 and 3 show that in all cases χ converges to the shear

direction of 0° as the shear flow becomes extremely strong. Smaller R makes χ converge more rapidly, and so χ curves of $R = 0.6$ are to be always a little below those of $R = 1$. When $R = 1$ and little or no electric field is applied, the saturated extent of Δn is not so complete even at the extremely strong shear field. The most significant feature in this region may be that Δn, for small R, has a remarkably small limiting value, as seen in the results of $R = 0.6$. This tells us that, at very strong flow fields, Δn is much influenced by the solute particle's shape and its limit value is determined mainly by R. Then respective dipoles bring up rather different dependencies on the electric field. When the permanent dipole is included, the results for $R = 1$ depend fairly strongly on the electric field at extreme α but all Δn curves of $R = 0.6$ converge to a unique limiting value. For the results with induced dipole, Δn in both cases of $R = 0.6$ and 1 depends on the electric field, but its extent of dependence is somewhat weak. Such dependencies of Δn on the electric field at extreme α are also found in the results for χ. Differences between dependencies of the electric field that respective dipoles show at extreme α can be explained as follows. The permanent dipole is electrically asymmetric, which causes effect of the electric field to vary only modestly, depending on R. Thus when R is small, the electric field effect due to the permanent dipole can be removed completely. Particles with the induced dipole alter their charge directions instantaneously during the rotary motion by the shear flow. Therefore, the induced dipole moment, irrespective of R, is difficult to be swamped completely, even for the strong shear flow.

Knowledge of two functions χ and Δn can contrarywise yield two Euler angles θ and ϕ averaged in the domain. To simplify matters, we restrict our attention to the cases that χ converges to 0° and Δn has a unique convergence limit. Such a state may be given more feasibly by extremely strong flow when the permanent dipole is included and R is small, as seen in cases of $R = 0.6$ of Fig. 2. Then the optical state depends solely on θ. When $\chi = \langle\phi\rangle = 0°$, Eq. (10) is reduced simply to $\Delta n/C = P_2^2$. Hence, from the Legendre polynomial relation,

$$\theta = \cos^{-1}\left(1 - \frac{\Delta n}{3C}\right)^{1/2}. \tag{14}$$

When the solute particle is a sphere ($R = 0$), Δn is always zero and $\langle\theta\rangle$ becomes 0° from Eq. (14). As R increases, Δn comes to have any finite value off zero and $\langle\theta\rangle$ increases accordingly. This means the solute particle tends to lie down along the flow direction. Though the above

TABLE I. Typical values of the field parameters and other variables in EHD experiment using m-cresol solution of poly-γ-benzyl-L-glutamate.

Operational conditions:	
Temperature $T = 25$ °C	
Shear rate $G = 400\ s^{-1}$	
Electric field $E_0 = 35$ kV/cm	
PBLG as a solute:	
M.W. = 236 000	
Radius of major axis, $a = 8.126 \times 10^{-8}$ m	
Radius of minor axis, $b = 9.1 \times 10^{-10}$ m	
Permanent dipole moment per unit volume $\mu_0 = 0.04365$ C m/m^3	
m-cresol as a solvent:	
Viscosity $\eta_0 = 0.126$ Pa s	
Dielectric constant of solvent $K_2 = 11.8$	
Dielectric ratio $q = 0.2$ roughly guessed	
Dimensionless parameters and other variables:	
$R = 0.999\ 75$	$\beta = 10.4$
$D_r = 337.0\ s^{-1}$	$\gamma^2 = 0.7368$
$\alpha = 1.187$	

explanation is restricted to a special limiting case, more general problems can also be managed in a similar way without further difficulties. In addition, Eq. (14) shows that $\Delta n/C = 3$ is the theoretical maximum value that can be obtained ultimately.

Thus far, we have dealt with the optical phenomena using *dimensionless* field parameters. Estimation of these parameters is needed to give the physical sense and intuition to the previous analyses. This is also required as a preliminary step to interpret experimental results already existing, or to prepare new experiments. Table I shows typical values that the dimensionless field parameters and other variables may have in EHD experiments using a well known m-cresol solution of PBLG. Each value of Table I was inferred from literatures or calculated based on the equations developed in this study. In EHD experiments, ranges of field strengths to be examined are largely restricted mainly due to the availability of the object macromolecules and the performance of the relevant apparatus. Modest values of the field parameters in Table I suggest EHD experiment at strong fields is not easy. Larger values of parameters, particularly for α, will be obtainable if higher molecular weight polymers are used. Even a larger value of the apparent sheer rate α may be obtained by using more concentrated solutions, but a different analysis is needed to consider the molecular interactions. Difficulties

related to the strong field problem are also incurred in EHD experiments using other synthetic polypeptides or biopolymers, too.

We have a particular interest in the rheo-optical behavior as a function of molecular weight of a polymer. Increase of MW of a polymer can be often interpreted as an increase of the aspect ratio r. In such a case, it can be assumed that the minor axis length of a rigid polymer is nearly constant and the increase of the major axis length corresponds to the increase of MW. Then, at specified experimental conditions, three field parameters can be represented as functions of aspect ratio. As r becomes large enough (roughly $r > 5$), each field parameter comes to have simple proportional relation to r, as follows:

$$\alpha \sim \frac{r^3}{\ln(2r) - 0.5}, \tag{15a}$$

$$\beta \sim r, \tag{15b}$$

$$\gamma^2 \sim r. \tag{15c}$$

Figure 4 shows the optical behaviors predicted for PBLG solutions with various molecular weights (M.W.) when the above assumption is satisfied that increases in r correspond roughly to increases in M.W. Here, based on the typical values of Table I, shear and electric fields of several strengths were chosen appropriately. As implied in Eqs. (15a) and (15b), use of polymers with large M.W. makes χ decrease and Δn increase according to their own dependencies on respective field parameters. Therefore, to successfully perform the EHD experiment at strong fields, molecular size and shape must be considered together with the field conditions. Close observation of Fig. 4 tells us rigid polymers of large M.W. in strong electric fields can be studied discriminently by the measurement of the birefringence Δn.

It can be said, from the preceding results and discussions, that problems with strong combined fields have their own characteristics in electrohydrodynamics. It is also conceived that a spheroid of revolution adopted in this article is a good model, moderately approximating a number of rigid macromolecules. Of course, analyses of the experimental data and the way to apply the theory can be altered to some extent according to the purpose of research and the choice of the sample solution.

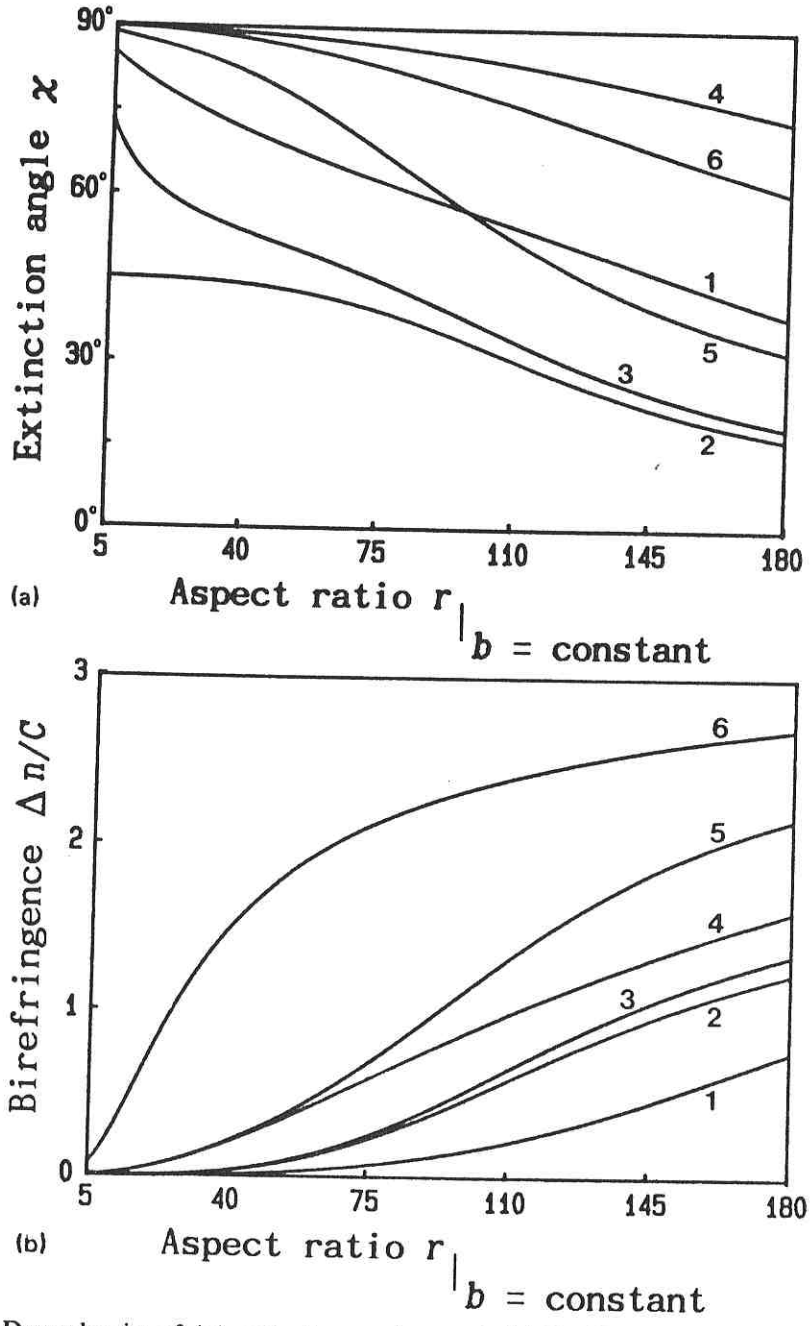

FIG. 4. Dependencies of (a) extinction angle χ and (b) birefringence $\Delta n/C$ on aspect ratio $r_{|b=\text{const}}$ when the minor axis b of the spheroid is constant. Combined external fields are as follows:

	1	2	3	4	5	6
Shear rate $G(s^{-1})$	100	400	400	50	400	400
Electric field E_0(kV/cm)	2	0	2	8	8	35

and other data except G and E_0 were taken from Table I.

CONCLUSION

When simultaneous shear and electric fields are applied to a dilute solution in which rigid macromolecules are soluble in a Newtonian solvent, its steady state optical behavior may be described uniquely. Macromolecules were modeled as rigid spheroids of arbitrary aspect ratio and both permanent and induced dipole moments were included. To solve the problem with arbitrary strength of fields, we have utilized the Galerkin method with spherical harmonics as basis functions and a specially designed numerical scheme to reduce the computation time significantly.

For more systematic interpretation, full ranges of the applied field strengths were divided into three regions according to their relative field strengths. Effect of the dimensionless shear rate α on the optical state was always related directly to the shape of molecules, that is, R. Over a wide range of the applied field strength, the extinction angle χ is influenced by the molecular shape. In particular, with increasing α, R had an opposite contribution to χ about the intersection in region 2 (the intermediate region). Birefringence Δn was little influenced by R until the shear flow became quite strong. As α goes to infinity, however, Δn depended significantly on R. When R was small, Δn even decreased and converged to a remarkably small limiting value. Respective effects of the permanent and induced dipoles on the optical state were not greatly distinguished for most field conditions which were explored. Merely beyond the considerable strength of shear flow, each dipole revealed its own characteristic combined with the geometric effect by R. Representative results for various coupled fields were also presented, including the saturation behaviors seen near extreme conditions. Most of the features seen at extremely strong shear fields were governed and characterized by severe RBM effect. Additionally it was shown, taking PBLG solutions with various M.W. as a concrete example, how theoretical results in this article are applicable to an analysis of a real system. (Present results would also be applicable to the needlelike cluster model, ferromagnetic fluids, transient problems, etc., without many difficulties.)

References

Arp, P. A., R. T. Foister, and S. G. Mason, "Some Electrohydrodynamic Effects in Fluid Dispersions," Adv. Colloid Interface Sci. **12**, 295–356 (1980).

Bird, R. B., R. F. Curtiss, R. C. Armstrong, and O. Hassager, *Dynamics of Polymeric Liquids* (Wiley, New York, 1987), Vol 2.

Frattini, P. L. and G. G. Fuller, "A Note on Phase-Modulated Flow Birefringence: A Promising Rheo-Optical Method," J. Rheol. **28**, 61–70 (1984).

Ikeda, S., "Orientation Birefringence of Macromolecular Solutions in Shear Flow and Electric Field," J. Chem. Phys. **38**, 2839–2844 (1963).

Johnson, S. J., P. L. Frattini, and G. G. Fuller, "Simultaneous Dichroism and Birefringence Measurements of Dilute Colloidal Suspensions in Transient Shear Flow," J. Colloid Interface Sci. **104**, 440–455 (1985).

Kamiyama, S. and A. Satoh, "Rheological Properties of Magnetic Fluids with the Formation of Clusters: Analysis of Simple Shear Flow in a Strong Magnetic Field," J. Colloid Interface Sci. **127**, 173–188 (1989).

Leal, L. G. and E. J. Hinch, "The Effect of Weak Brownian Rotations on Particles in Shear Flow," J. Fluid Mech. **46**, 685–703 (1971).

Leal, L. G. and E. J. Hinch, "The Rheology of a Suspension of Nearly Spherical Particles Subject to Brownian Rotations," J. Fluid Mech. **55**, 745–765 (1972).

Meeten, G. H., *Optical Properties of Polymers* (Elsevier, London, 1986), Chap. 3, pp. 101–124.

Melcher, J. R. and G. I. Taylor, "Electrohydrodynamics: A Review of the Role of Interfacial Shear Stresses," Ann. Rev. Fluid Mech. **1**, 111–146 (1969).

Mukohata, Y., S. Ikeda, and T. Isemura, "The Electric-Streaming Birefringence of Poly-γ-benzyl-L-glutamate in m-Cresol," J. Mol. Biol. **5**, 570–573 (1962).

Okagawa, A., R. G. Cox, and S. G. Mason, "Particle Behavior in Shear and Electric Fields. VI. The Microrheology of Rigid Spheroids," J. Colloid Interface Sci. **47**, 536–567 (1974).

O'Konski, C. T., ed., *Molecular Electro-Optics* (Dekker, New York, 1976), Parts 1 and 2.

Park, O. O., "Electrohydrodynamics of Rigid Macromolecules with Permanent and Induced Dipole Moments," J. Rheol. **32**, 511–531 (1988).

Stewart, W. E. and J. Sørensen, "Hydrodynamic Interaction Effects in Rigid Dumbbell Suspensions. II. Computations for Steady Shear Flow," Trans. Soc. Rheol. **16**, 1–13 (1972).

Strand, S. R., S. Kim, and S. J. Karrila, "Computation of Rheological Properties of Suspensions of Rigid Rods: Stress Growth after Inception of Steady Shear Flow," J. Non-Newtonian Fluid Mech. **24**, 311–329 (1987).